Biosensors and Bioelectronics 53 (2014) 90–98

Contents lists available at ScienceDirect

Biosensors and Bioelectronics

journal homepage: www.elsevier.com/locate/bios

Target-induced electronic switch for ultrasensitive detection of Pb^{2+} based on three dimensionally ordered macroporous Au–Pd bimetallic electrode

Xiaojun Chen [a,b,*], Rong Tian [a], Qi Zhang [c], Cheng Yao [a,*]

[a] College of Sciences, Nanjing University of Technology, Nanjing 211816, PR China
[b] State Key Laboratory of Materials-Oriented Chemical Engineering, Nanjing University of Technology, Nanjing 210009, PR China
[c] Nanjing Sichuang Biotechnology Co. Ltd., Nanjing 211800, PR China

ARTICLE INFO

Article history:
Received 13 June 2013
Received in revised form
11 September 2013
Accepted 12 September 2013
Available online 26 September 2013

Keywords:
Three dimensional ordered macroporous materials
Au–Pd bimetallic electrode
Methylene blue modified carbon nanotubes
DNAzyme biosensor
Lead detection

ABSTRACT

A novel strategy for selective and sensitive amperometric detections of Pb^{2+} was proposed based on the three dimensional ordered macroporous (3DOM) Au–Pd bimetallic electrode and target-induced methylene blue-single walled carbon nanotubes (MB-SWCNTs) as signal reporter. A DNA biosensor was fabricated by immobilizing capture probe DNA on the 3DOM Au–Pd bimetallic electrode, which further hybridized with the reporter DNA loaded on the MB-SWCNTs adduct upon the exposure of Pb^{2+}, inducing measurable electrochemical signal. Due to the dramatic signal amplification by the enhanced immobilization of DNA on the surface of 3DOM Au–Pd bimetallic electrode and MB-SWCNTs, coupling the low background signal produced by blank solution, ultra-low level (1×10^{-19} M) of Pb^{2+} could be detected. Under the optimal conditions, the electrochemical signal of the MB increased with the increasing Pb^{2+} concentration, exhibiting a linear response in the range of 1×10^{-17}–1×10^{-4} M. Furthermore, with the application of Pb^{2+} dependent DNAzyme, the proposed sensing system demonstrated high selectivity. This work represented a promising potential for on-site testing Pb^{2+} in real drinking water and serum sample analysis.

1. Introduction

DNAzyme, artificial deoxyribozyme, can catalyze the cleavage of their substrates in the presence of a particular metal ion, showing extra-high metal-binding affinity and specificity. At present, many different DNAzymes have been screened, such as Mg^{2+}-dependent RNA-cleaving DNAzyme (Gao et al., 2012), histidine-dependent DNAzyme (Li et al., 2011), Cu^{2+}-dependent RNA-cleaving DNAzyme (Li et al., 2013), DNA ligase DNAzyme (Dong et al., 2013), and porphyrin metallation-catalyzing DNAzyme (Zhang et al., 2013a,b). Among them, the Pb^{2+}-dependent RNA-cleaving DNAzyme was firstly and widely used, and its catalytic action was 100-fold that of the noncatalyzed process (Kruger et al., 1982; Li and Lu, 2000). The reason why the detection of Pb^{2+} content has been focused on for decades of years is that the lead pollution is so dangerous to the environment and human health. Although the cutoff value of Pb^{2+} ion defined by the US Environmental Protection Agency (EPA) in the drinkable water is 72 nM, it is still very harmful to the intellectual development of children. In the year of 1997 and 1998, the US EPA defined the ceiling of blood lead levels (BLLs) as 0.48 nM. Recent studies have shown that even lower BLLs may be considered potentially hazardous (Jusko et al., 2008; Huang et al., 2012). Therefore, it is essential to develop sensors for ultrasensitive detection of Pb^{2+}.

During the past few years, several electrochemical studies based on Pb^{2+}-specific DNAzymes have shown that electrochemical methods possessed high sensitivity over optical methods. Xiao et al. proposed a simple electrochemical approach based on the Pb^{2+}-requiring DNAzyme, with the detection limit of 0.3 μM, which could satisfy the routine monitoring of Pb^{2+} levels in food and environmental samples (Xiao et al., 2007). Zhang's group introduced nanoporous Au electrode to immobilize more capture probe DNAs, and used a multifunctional DNA–Au bio bar code as a means of amplification, enabling the detection limit to be 28 aM (Hu et al., 2008). Tian et al. designed a novel Pb^{2+}-specific DNAzyme functionalized Au nanoparticles to achieve signal enhancement, obtaining the detection limit of 0.028 nM (Yang et al., 2010). Tang and his coworkers constructed a magneto-controlled electrochemical DNA biosensor for the detection of Pb^{2+}, coupling a Pb^{2+}-specific DNAzyme with DNA based hybridization chain reaction (HCR), achieving a detection limit of 37 pM

* Corresponding authors at: College of Sciences, Nanjing University of Technology, Nanjing 211816, PR China. Tel./fax: +86 25 858139527.
E-mail addresses: chenxj_njut@126.com (X. Chen), yaochengnjut@163.com (C. Yao).

0956-5663/$ - see front matter © 2013 Elsevier B.V. All rights reserved.
http://dx.doi.org/10.1016/j.bios.2013.09.028

(Zhuang et al., 2013). Zhang et al. developed another electrochemical sensing system based on Pb^{2+}-specific DNAzyme and rolling circle amplification (RCA), with the detection limit of 7.8 pM (Tang et al., 2013). Among these methods, the electrochemical biosensors can achieve ultrasensitive detection for Pb^{2+} with the introduction of amplification strategies, and possess many advantages, such as good portability, low cost and simple instrumentation. Despite many advances in this field, a higher sensitivity is still desired for complex biological or environmental samples detection to ensure large signal-to-noise ratios. In addition to the low concentrations of heavy metal ions, real samples are usually complicated by the presence of other ions, making the determination of Pb^{2+} a difficult task.

Recent reports show that the use of nanostructured materials can lead to a miniaturization of functional units and the development of novel electrochemical systems. For example, Au nanomaterials have been widely used for promoting the electron transportation or as carriers for loading numerous signal tags with acceptable function of signal amplification. Nowadays, Au-based bimetallic nanomaterials, such as the combination of Au with Ag (Dallaire et al., 2012), Pd (Qian et al., 2010), Ru (Yi et al., 2010) and Pt (Yang et al., 2012), are attracting increasing attention because they can not only incorporate properties of the individual constituents but also exhibit an enhancement in specific properties owing to the synergistic effects and the rich diversity of the compositions. In these works, bimetallic electrodes typically provide a rapid response, good stability, electrocatalytic capability and better resistance to deactivation for the selected target detection. In order to further improve the electrochemical behavior of biosensors, three dimensionally ordered macroporous (3DOM) modified electrodes have been constructed, which can ensure the accessibility of reactants to the active surface sites of electrodes, increasing both the mass transport of reactant and mass-normalized activity. Especially, the 3DOM Au nanostructured surfaces have been widely used in biosensors, due to their fascinating properties such as well-ordered pore structure, high-specific pore volume as well as high conductivity, stability and biocompatibility (Gamero et al., 2013; Zhou et al., 2010; Chen et al., 2008).

Here, we firstly reported an ultrasensitive electrochemical detection of Pb^{2+} by coupling the signal amplification strategy of 3DOM Au–Pd bimetallic electrode and single-walled carbon nanotubes (SWCNTs) labels with substrate DNAs as a recognition element. The characteristics consisted in this assay protocol mainly including (1) the Pd was selected as the combination of Au because of its relatively higher abundance and lower cost, and 3DOM Au–Pd alloy also had high electronic conductivity, which could accelerate response time and widen linear range; (2) the Au nanoparticles combined magnetic beads (GMB) were used as not only an immobilization substrate to enhance the DNAzyme immobilization amount, but also a separation tool to remove the dispatched DNAs; and (3) SWCNTs are chosen as the supporting materials for single-stranded DNAs (ssDNAs) and electroactive methylene blue (MB) to enhance the electrochemical signals.

2. Experimental

2.1. Materials and chemicals

High-performance liquid chromatography (HPLC) purified DNA oligonucleotides containing the Pb^{2+}-specific DNAzyme (DNA2) and DNA3 captures were obtained from Sangon Biotech. Co., Ltd. (Shanghai, China). The DNA substrate (DNA1) with a single, sessile ribonucleoside adenosine (rA) (represent in red font in Scheme 1) was purchased from TaKaRa Biotech. Co., Ltd. (Dalian, China) and purified by RNase Free HPLC by the company. The sequences of oligonucleotides are listed as follows:

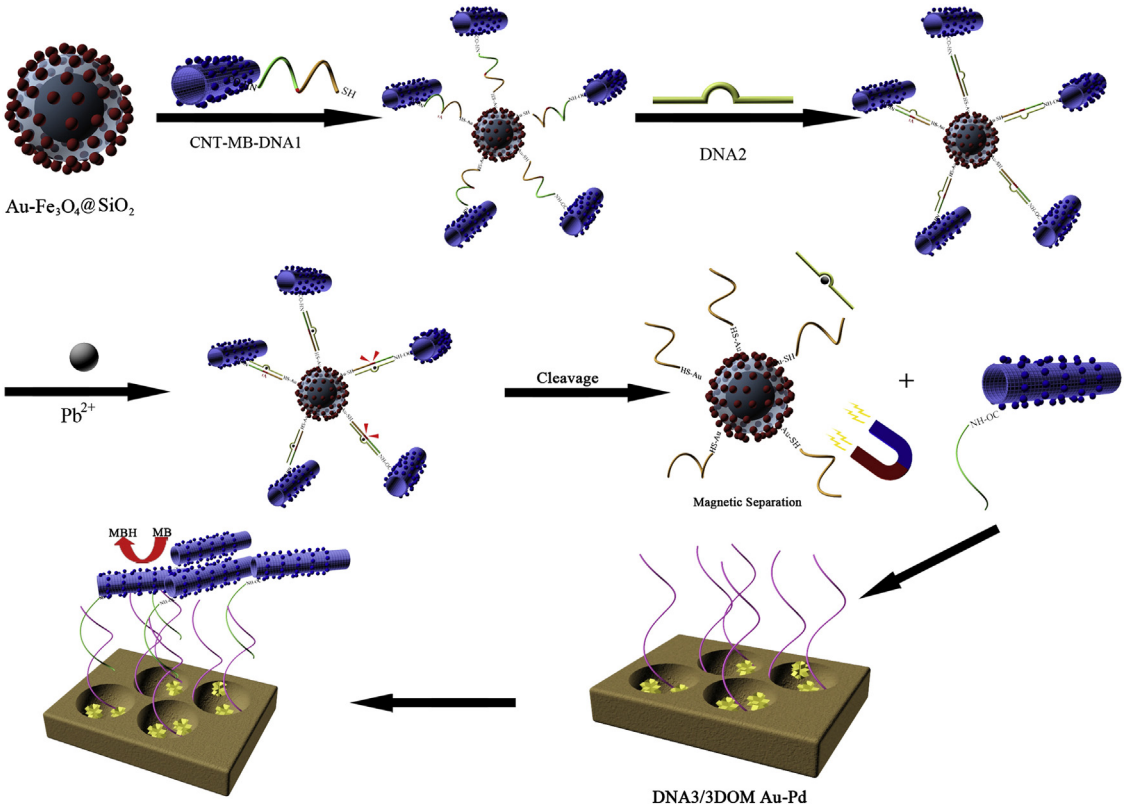

Scheme 1. Measurement protocol of the DNAzyme-based sensor for Pb^{2+} detection. (For interpretation of the references to color in this figure caption, the reader is referred to the web version of this paper.)

DNA1: 5′-NH_2-T_8ACTCACTAT ***rA*** GGAAGAGATG-T_{12}-HS-3′
DNA2: 5′-CATCTCTTCTCCGAGCCGGTCGAAATAGTGAGT-3′
DNA3: 5′-HS-ATAGTGAGTAAA-3′

6-Mercaptohexanol (MCH), MB, poly (diallyldimethylammonium chloride) (PDDA, 20 wt.%) and diethyl pyrocarbonate (DEPC) were purchased from Sigma Chemical Co. (St. Louis, MO, USA). Stock solution of 3 wt.% PDDA was prepared in double distilled water with Tris and NaCl. The supporting electrolyte phosphate buffer saline (PBS, 0.1 M) was prepared by mixing the stock solutions of KH_2PO_4 and K_2HPO_4, and adjusted to appropriate pH by the addition of 0.1 M NaOH or H_3PO_4 solution. Shortened carboxylated SWCNTs were obtained from Nanjing XFNano Materials Tech. Co., Ltd. The mono-dispersed silica spheres with the diameters of 500 μm were obtained from Alfa Asear. Glutaraldehyde (GA, 25 wt.%) was supplied by Chengdu Kelong Chemical Reagents. Ferric chloride hexahydrate ($FeCl_3 \cdot 6H_2O$), polyethylene glycol (PEG) 10,000, sodium acetate anhydrous (NaAc), potassium ferricyanide ($K_3[Fe(CN)_6]$), potassium ferrocyanide ($K_4[Fe(CN)_6]$) and potassium chloride (KCl) were all purchased from Shanghai Linfeng Chemical Reagent Co., Ltd., China. The supporting electrolyte solution of cyclic voltammetry (CV) and electrochemical impedance spectroscopy (EIS) measurements was 0.1 M KCl solution containing 5 mM $[Fe(CN)_6]^{3-/4-}$ (1:1). Chloroauric acid hydrated ($HAuCl_4 \cdot 4H_2O$) and potassium tetrachloropalladate (K_2PdCl_4) were purchased from Nanjing Chemical Reagent Co. Ltd., China. Other reagents were of analytical grade and used without further purification. Double distilled water was used throughout the experiments.

Before the experiment for Pb^{2+} detection, it is important to indicate that the DNA1 is a DNA/RNA chimera with ribonucleotide adenosine (rA) and is not stable and easily degradable like RNA; thus, great care should be taken to avoid inadvertently introducing RNases into the DNA1 solution during operation. To create and maintain an RNase-free environment, solutions (water and other solutions) were treated with 0.1% DEPC. When preparing Tris buffers, water should be treated with DEPC first before dissolving Tris to make the appropriate buffer. DNA immobilization buffer involved in this work was composed of 300 mM NaCl and 25 mM Tris-acetate (pH 8.0). The stock solution of Pb^{2+} (1 mM) was prepared by dissolving $Pb(Ac)_2 \cdot 3H_2O$ in 10% HAc; further dilution was performed with 50 mM Tris-acetate (0.5 M NaCl, pH 8.0).

The serum samples from different persons were provided by Jiangsu Center for Clinical Laboratory (JSCCL), and the values of Pb^{2+} in the serum samples had been detected by automatic biochemical analyzer.

2.2. Apparatus

The structures, surface morphology and elemental composition of the 3DOM Au–Pd electrode were characterized by Philip-X′Pert X-ray diffractometer taken with a Cu KR X-ray source, field-emission scanning electron microscopy (FESEM, Hitachi S4800) and energy-dispersive X-ray spectroscopy (EDS Falcon 60S, EDAX Inc.), respectively. The morphology and composition of MB combined SWCNTs were characterized by transmission electron microscopy (TEM, JEOL JEM-200CX) and by Fourier transform infrared (FT-IR) spectroscopic measurements (Bruker, VECTOR22) using KBr pressed disks. UV–Vis spectra were recorded on Agilent UV–Vis spectrophotometer. Zeta potential analysis was performed with a PALS Zeta Potential Analyzer, version 3.43 (Brookhaven Instruments Corp.). CV, EIS and amperometric measurements were performed using a CHI660D electrochemical workstation (Shanghai CH Instruments, China). A three-compartment electrochemical cell contained a saturated calomel reference electrode (SCE) against which all potentials were measured in this paper, a platinum wire auxiliary electrode and the 3DOM Au–Pd modified Au disk electrode (ϕ=2 mm) as working electrode. The sensor responses were measured as the difference between total and background currents.

2.3. Fabrication of 3DOM Au–Pd electrode

Au substrates were provided by Shanghai Institute of Microsystem and Information Technology, Chinese Academy of Sciences. They were prepared by sputtering a 200 nm thick Au top layer onto the quartz wafers, which was previously coated with a few nanometers of Cr adhesion layer under vacuum. The preparation of the 3D silica close-packed colloidal crystal modified Au electrode with controlled area (ϕ=2 mm) was similar to our previous work (Chen et al., 2008). In brief, a clean gold substrate was immersed vertically into a diluted SiO_2 suspension, which was prepared by ultrasonic dispersing 0.35 g SiO_2 spheres into a 60 mL water–ethanol mixture (10/90, v/v). A temperature controlled vibration-free furnace chamber was used to keep the temperature at 35 °C. Two days later, a 3D silica close-packed colloidal crystal formed through solvent evaporation. After that, the silica crystal template was sintered at 250 °C to ensure its mechanical strength. The electrode area was controlled by an apertured insulating tape covering the edge of SiO_2 layers and was determined to be 0.07 cm^2. Then the Au–Pd bimetallic alloy was first prepared by controlled co-reduction deposited into the template interspaces. In a typical synthesis, a 3D silica modified Au electrode was immersed in a 0.1 M $HClO_4$ solution containing 2 mM $HAuCl_4 \cdot 4H_2O$ and 2 mM K_2PdCl_4 for 5 min, followed by electrodeposition of Au–Pd at a potential of 0 V as 0.17 C charge was passed during electro-deposition. To ensure that the electrons could only be used to reduce Au(III) and Pd(II) ions, the electrolyte solution was deaerated with N_2 and N_2 flowed over the solution throughout the whole process. After electro-deposition, an ordered pore array was obtained by dissolving the template in aqueous HF (5%) for 60 s.

2.4. Fabrication of DNA3 modified 3DOM Au–Pd electrode

After the preparation of the 3DOM Au–Pd electrode, it was electrochemically cleaned by cyclic scanning with a potential range of 0–1.6 V in 0.5 M H_2SO_4 at a scan rate of 100 mV s^{-1} until a reproducible CV was obtained. Then, the freshly prepared 3DOM Au–Pd electrode was immediately immersed into an immobilization buffer containing 6 μM DNA3 for 12 h, and the whole system was put at 37 °C in a homothermal water bath chamber with 100% humidity to avoid dehydration. The DNA3-modified 3DOM Au–Pd electrode was further treated with 1 mM MCH for 2 h to obtain a well-aligned DNA monolayer, followed by washing with PBS buffer to remove unspecific adsorbed DNA.

2.5. Fabrication of the biocomposite of Au–SiO_2@Fe_3O_4 with DNA1–MB-SWCNTs

Since the carboxylated SWCNTs were negatively charged with ζ-potential of −17.68 mV, the positively charged MB molecules with ζ-potential of +14.66 mV could be absorbed onto the surface of SWCNTs. One milligram MB was added into the 2 mL water dispersion containing 1 mg SWCNTs, and the whole solution was kept at room temperature for 1 h under stirring. The formed MB-SWCNTs' adducts were collected by centrifugation at 9000 rpm for 4 min. After thoroughly washed with double distilled water to remove the non-absorbed or loosely adsorbed MB, the MB-SWCNTs' adducts were obtained. Afterwards, GA (2.5 wt.%, 10 μL) and MB-SWCNTs (0.5 mg mL^{-1}, 10 μL) were added into a 50 μL immobilization buffer containing 10 μM DNA1. The mixture was incubated for 12 h at room temperature under gentle stirring. The DNA1 was covalently combined onto the surface of MB-SWCNTs through the linkage of GA and 5′ terminal amino groups.

The surplus of DNA1 was washed away by PBS buffer for three times. Then, DNA1–MB-SWCNTs were re-suspended in 50 μL of 0.1 M PBS (1 M NaCl, pH 7.4).

Au–Fe_3O_4@SiO_2 core/shell composite was prepared similar to our previous work (Chen et al., 2011). Fifty microliters of above-mentioned DNA1–MB-SWCNTs was added into 1 mL of a suspension of 50 mg mL^{-1} Au–Fe_3O_4@SiO_2 in double distilled water. The mixture was incubated for 12 h at room temperature under gentle stirring. DNA1 was chemi-absorbed to Au–Fe_3O_4@SiO_2 via a 3′ terminal thiol and then the biocomposite of Au–SiO_2@Fe_3O_4 with DNA1–MB-SWCNTs was obtained. The redundant DNA1–MB-SWCNTs were removed by magnetic separation.

2.6. Fabrication of Pb^{2+}-specific DNAzyme-based sensor

The designed strategy of the DNAzyme based sensing system was depicted in Scheme 1. Firstly, the biocomposite Au–SiO_2@-Fe_3O_4–DNA1–MB-SWCNTs was re-suspended in 100 μL containing 6 μM DNA2 to make it hybridize with DNA1 in a water bath at 90 °C for 10 min. After that, the hybridization process was further carried out at room temperature for 12 h. The obtained magnetic beads and MB-SWCNTs functionalized DNA1/DNA2 (catalytic/substrate) strands were separated and dispersed in 1 mL of 50 mM Tris-acetate (0.5 M NaCl, pH 8.0) buffer for further use.

In the absence of Pb^{2+}, the DNA2 was inactivated, so the substrate strand could not be cleaved. However, in the presence of Pb^{2+}, DNA2 catalyzed hydrolytic cleavage of the DNA1 strand at the scissile rA (red font). The DNA1 was divided into two fragments and DNA2 was released. One fragment linked with Au–SiO_2@Fe_3O_4 was removed by magnetic separation, and the other fragment combined with MB-SWCNTs gained the chance of hybridization with DNA3 on the 3DOM Au–Pd electrode surface. As a result, the DNA–MB-SWCNTs complexes were immobilized onto the electrode surface, thus, the faradaic current of MB could be investigated. The current intensity increased with increasing Pb^{2+} concentration. In this way, the concentration of Pb^{2+} in solution could be obtained indirectly.

3. Results and discussion

3.1. Preparation and characterization of 3DOM Au–Pd modified electrode

Apart from excellent biocompatibility, Au-based 3DOM structure is a good candidate for fabricating biosensors, because its large surface area can increase significantly detection signals (Wei et al., 2011; Xu et al., 2009; An et al., 2013). An ideal method of developing 3DOM metallic materials with controlled size and spatial arrangement of pores is to use colloidal crystal films as templates for subsequent electro-deposition (Wijnhoven et al., 2000). Here, a 3DOM Au–Pd bimetallic film modified Au electrode was prepared through electro-controlled co-reduction method using the ordered colloidal assembly of silica spheres as sacrificial template. To the best of our knowledge, there are no previous reports on the preparation of 3DOM Au–Pd bimetallic film by this technique. Au–Pd was simultaneously electro-deposited into the interspaces of the silica-crystal template at a potential of 0 V. After 0.17 C charges were passed during electro-deposition, the thickness of bimetallic Au–Pd film nearly equaled to the radius of silica sphere. And then, a single-layered macroporous Au–Pd film was obtained followed by removal of the silica template with aqueous HF. As shown in the SEM characterization of Fig. 1A, the morphology of 3DOM Au–Pd film was hexagonally close-packed, indicating an inverse opal structure of a continuous 3DOM nature. The average diameter of the pores was about 350 nm and the average wall thickness of the pores was about 140 nm. The EDS pattern (inset of Fig. 1A) displayed the typical diffractions of Au and Pd, revealing the successful synthesis of Au–Pd bimetallic structures under proposed conditions (Note: the ITO electrode was used here as the substrate of electro-depositing

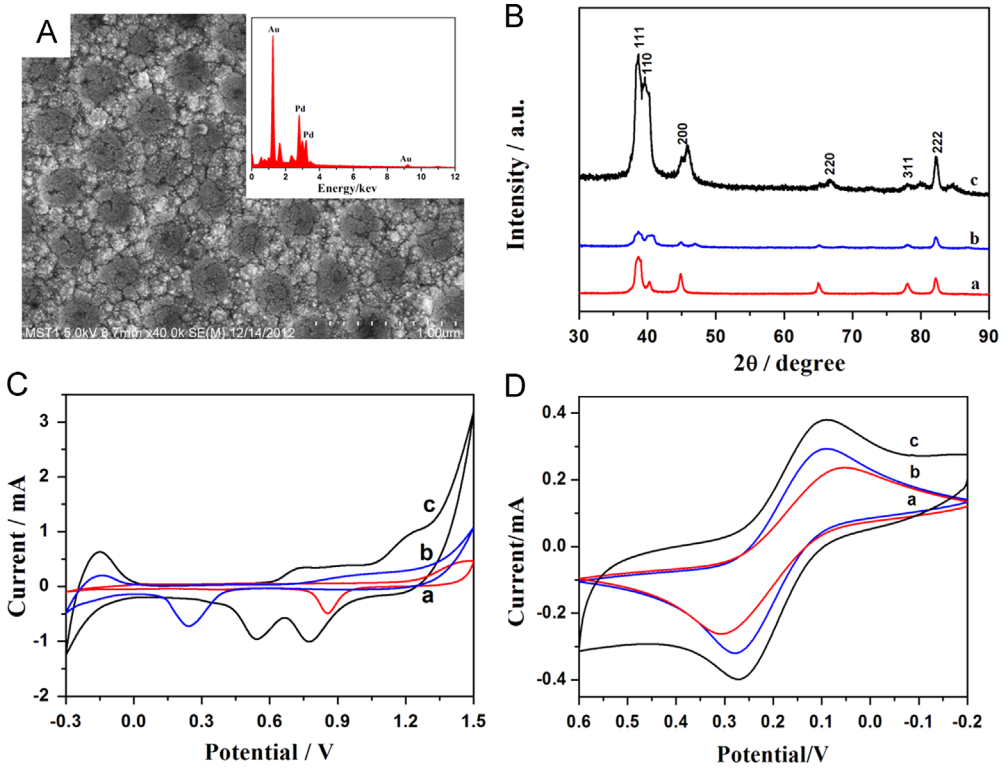

Fig. 1. (A) Magnified SEM image of the as-synthesized 3DOM Au–Pd; (B) XRD patterns; (C) CVs in 0.5 M H_2SO_4 at a scan rate of 50 mV s^{-1}; (D) CVs in 5 mM $[Fe(CN)_6]^{3-/4-}$ (1:1) solution containing 0.1 M KCl at a scan rate of 100 mV s^{-1} of (a) 3DOM Au, (b) 3DOM Pd and (c) 3DOM Au–Pd film. Inset: EDS pattern of 3DOM Au–Pd.

Au–Pd.) The EDS analysis indicated that the atomic ratio of Au:Pd was approximately 50.58:49.42, nearly 1:1 on the 3DOM Au–Pd electrode. Since the total electro-deposition charge was selected as 0.17 C, the allotted charges to Au and Pd were about 0.1 C and 0.07 C in the equimolar Au(III)/Pd(II) bath, respectively.

To obtain the further crystallographic information of the 3DOM Au–Pd film, an XRD measurement was conducted. The XRD patterns for 3DOM Au (curve a), 3DOM Pd (curve b) and 3DOM Au–Pd (curve c) films are all shown in Fig. 1B. Sharp and well defined peaks were observed for 3DOM Au–Pd at 2θ values of 38.7, 40.7, 44.8, 65.1, 78.4 and 82.2° corresponding to the (111), (110), (200), (220), (311) and (222) crystal orientations of the face-centered cubic crystal structure, respectively. The diffraction peaks for Au and Pd planes appeared at the similar 2θ values assuming that no alloy has been formed between Au and Pd (Datta et al., 2011). The average crystal size of Au–Pd bimetallic particles, which combined together to form 3DOM Au–Pd nanostructures, were determined from the full-width at half maximum (FWHM) of the (222) plane using the Debye–Scherer equation and the crystallite sizes were found to average 17.4 nm.

Fig. 1C depicts CV of the 3DOM Au–Pd in 0.5 M H_2SO_4 solution at a scan rate of 50 mV s^{-1} (curve c). For comparison, the CVs of 3DOM Au and 3DOM Pd with the same molar amount of electro-deposited metal were also presented as curves a and b, which meant the deposition charges were about 0.2 C and 0.15 C, respectively. All of these three 3DOM electrodes had the same geometric surface area. In the case of the 3DOM Au, a notable signal ascribed to the typical reduction of Au oxide was observed at around +0.86 V versus SCE (curve a). Differently, the 3DOM Pd provided a reduction peak of Pd oxide at +0.24 V. Another sharp peak was also observed below 0 V, owing to hydrogen adsorption–desorption at the 3DOM Pd surface (curve b). As for the 3DOM Au–Pd, the Pd peak overlapped with the Au peak at +0.54 V and +0.77 V, respectively. We speculated that the 3DOM Au–Pd bimetallic structure was the intermediate between simple 3DOM Au and 3DOM Pd films, thus the reduction peaks were obtained at +0.54 V and +0.77 V, respectively. Another expanded sharp peak at −0.16 V was observed, relating to the hydrogen adsorption–desorption responses on the electrode surface (curve c). Besides, the results of CVs in the ferricyanide system, as illustrated in Fig. 1D, demonstrated that the proposed 3DOM Au–Pd could exhibit enhanced performance for promoting electron transfer on the electrode/electrolyte interface in comparison with the 3DOM Au and 3DOM Pd. The peak potential difference (ΔE_p) for the 3DOM Au–Pd (170 mV) was also found to be smaller than that for the 3DOM Au (250 mV) and 3DOM Pd (190 mV). The 3DOM Au–Pd electrode exhibited the promotion of electron transfer in comparison with the 3DOM Au and 3DOM Pd, which might resulted from the formation of hetero-metallic bond between Au and Pd nanoparticles as they were distributed homogenously on the substrate (Zhang et al., 2013a,b). Owing to the small spacing between individual Au and Pd nanoparticles compared with the size of nanoparticles, the construction of electrode interface having micro/nanoscale chemical architectures could result in the overlapping diffusion zones and resultant planar diffusion to the array. The inter-metallic charge transfer or orbital hybridization would drastically enhance the electrochemical performance (Gholivand and Azadbakht, 2012).

3.2. Characterization of MB-SWCNTs adduct

Highly sensitive bio-assays have been usually found using labeled detection, and the label is frequently an enzyme which can generate an electroactive species in the presence of substrate. Although such approaches provide high sensitivity, the deterioration of enzyme activity over time can be problematic. Alternatively, metal nanoparticles or redox mediators can provide labels of greater stability. Here, SWCNTs were used as ideal carriers to attach MB redox molecules through the strong π–π stacking adsorption between them (Yan et al., 2005). Fig. 2A shows the absorption spectra of a 3.47×10^{-6} M MB solution before exposure of the solution to SWCNTs and then after exposure and removal of the SWCNTs by filtration. The peak at 664 nm and shoulder at 612 nm are consistent with previous reports, and the shoulder has been attributed to the presence of MB dimers (Yan et al., 2005; Sagara and Niki, 1993). Taking the extinction coefficient for MB as 6.25×10^4 M^{-1} cm^{-1} (Yusuf et al., 2005), the decrease in absorbance of 0.08 after SWCNTs exposure corresponded to the removal of 1.15×10^{-6} mol MB by 1 mg SWCNTs, i.e., an MB loading on the SWCNTs of 1.15×10^{-3} mol g^{-1}. The loading capacity was similar with the result of literature (Chunglok et al., 2011), which was calculated by the same method.

Fig. 2B shows the FT-IR spectra of SWCNTs, MB and MB-SWCNTs. Curve a was the FT-IR spectrum of the SWCNTs with oxygen-containing moieties, such as carboxylic acid groups, at the ends of the nanotubes. The bands at 1702 and 1637 cm^{-1} were assigned to the C=O stretch mode of carboxylic acid and the stretching mode ν(C=O) of quinine groups produced at the nanotube ends, respectively (Cai et al., 2002). The band at 1618 cm^{-1} was attributed to the stretching mode ν(C=C) of double bonds in the nanotube backbone near the functionalized carbon atoms (Mawhinney et al., 2000). The FT-IR spectrum of free MB (curve b) exhibited its ring stretch at 1600 cm^{-1}, the symmetric stretch of C–N at 1396 cm^{-1}, and symmetric deformation of $-CH_3$ at 1363 cm^{-1} (Imamura et al., 2002). Compared with SWCNTs and free MB, the FT-IR spectrum of MB-SWCNTs (curve c) was substantial, and some group adsorption peaks of MB were changed upon its adsorption onto the SWCNTs. The ring stretching band was probably shifted to 1617 cm^{-1} and the symmetric stretch of C–N at 1398 cm^{-1} almost disappeared after its adsorption onto the SWCNTs, implying that this stretch may be largely broadened by the strong interaction between MB and the SWCNTs.

Fig. 2C depicts the CVs of the MB-SWCNTs/glassy carbon electrode (GCE) in PBS at various scan rates. As shown, the linear scan rate–peak current relationship in a range from 10 to 100 mV s^{-1} indicated surface-confined process, which required the redox coverage to be not much greater than a single monolayer.

Further study was performed to investigate the pH-dependence of the response of MB in the MB-SWCNTs adduct. CVs of MB-SWCNTs/GCE in 0.1 M PBS (0.1 M KCl) recorded from pH 4.0 to 9.0 at a scan rate of 50 mV s^{-1} are shown in Fig. 2D. The redox current increased from pH 4.0 and reached a maximum at pH 7.0, the current response was found to decrease from pH 7.0 to 9.0. The apparent formal potential shifted by a nearly ideal −60 mV/pH unit, indicating a reversible two electron transfer coupled with a two proton transfer electrochemical reduction process of MB over the entire pH range (Ceres et al., 2007). The reaction was as follows: $MBH^+MB+2H^+ +2e$. Since the buffer solution of pH 7.0 has the maximum signal response, 0.1 M PBS (0.1 M KCl) with pH 7.0 was chosen as the supporting electrolyte.

3.3. Characterization of the 3DOM Au–Pd based DNA biosensor

The different steps of the modified electrode surface could be characterized by faradic EIS. Fig. S2A shows the Nyquist plots of impedance spectra at different electrode surfaces in 0.1 M KCl solution containing 5 mM $Fe(CN)_6^{3-/4-}$. To obtain more information from EIS results, the working electrode was modeled by the equivalent circuit, as shown in the inset of Fig. S2A, which was used to fit the EIS data. The change in the diameter of the semicircle reflected the change in the interfacial charge-transfer resistance (R_{ct}). In addition to R_{ct}, the equivalent circuit contains

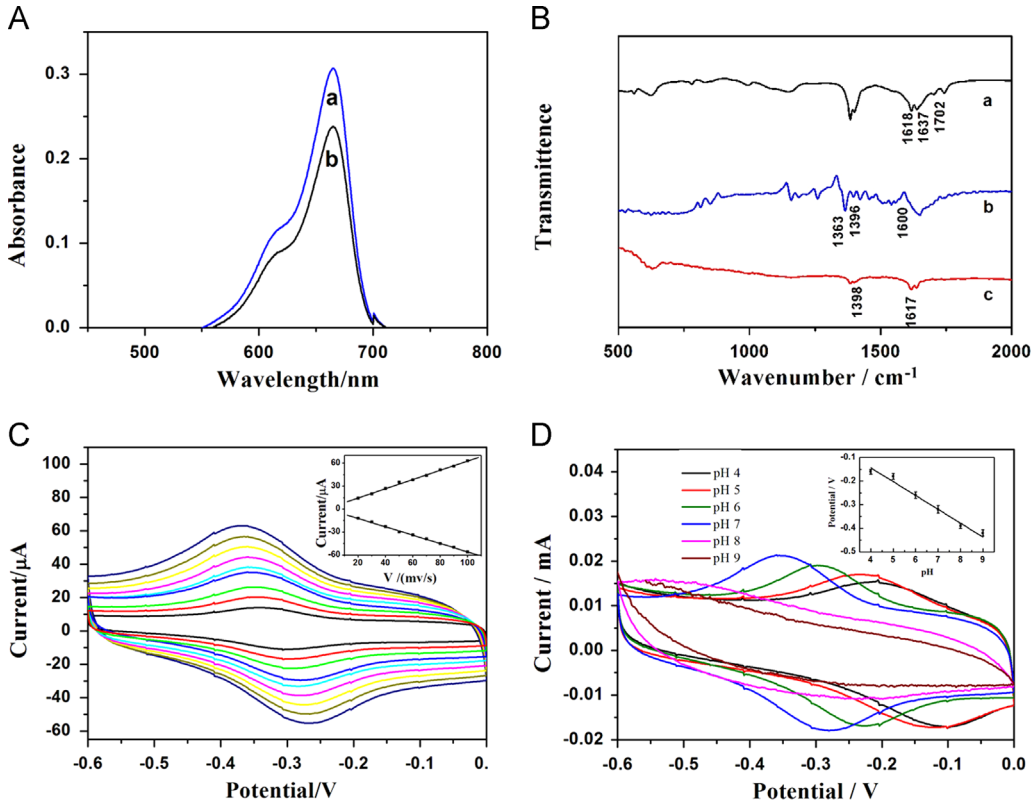

Fig. 2. (A) UV–Visible absorbance spectra of (a) 3.47×10^{-6} M MB in deionised water and (b) the same solution after exposure to 1 mg SWCNTs for 2 h followed by removal of the SWCNTs by filtration. (B) FT-IR spectra of SWCNTs (a), free MB (b) and MB-SWCNTs (c). (C) CVs of MB-SWCNTs/GCE at scan rates (inner to outer) 10, 20, 30, 40, 50, 60, 70, 80, 90, and 100 mV s^{-1}. Inset shows plots of anodic and cathodic peak currents versus potential scan rate. Electrolyte: 0.1 M pH 7.0 PBS+0.1 M KCl. (D) CVs of MB-SWCNTs/GCE in 0.1 M PBS (0.1 M KCl) at pH values from 4.0 to 9.0, scan rate: 50 mV s^{-1}.

R_s that is the electrolyte solution resistance, the Warburg impedance Z_w and the constant phase element related to double layer capacitance C_{dl}. For the 3DOM Au–Pd film, the value of R_{ct} was 20 Ω, revealing nearly a straight line, which indicated that the electrons on the surface of the electrode transport very rapidly. After the immobilization of DNA3, the value of R_{ct} increased to 106 Ω, attributing to the fact that negative charges of the DNA phosphate backbone prevent redox of $Fe(CN)_6^{3-/4-}$ approaching the electrode surface. In addition, the fractional surface coverage (θ) presented the extent of DNA3 immobilized on the electrode, which could be calculated by the following formula, $\theta = 1 - (R_{ct(Bare)}/R_{ct(DNA3)}) \times 100\%$, where $R_{ct(Bare)}$ and $R_{ct(DNA3)}$ were the electron transfer resistance values of bare 3DOM Au–Pd electrode and DNA3 modified 3DOM Au–Pd electrode, respectively. Then, the θ value was estimated as 81.1%. After the remaining active sites on the electrode surface were passivated by MCH, the R_{ct} value increased to 1549.7 Ω. Upon the addition of 0.1 nM Pb^{2+}, the MB-SWCNTs combined DNA was hybridized with DNA3, and the R_{ct} increased greatly to 1960.2 Ω, due to the large amount of DNA linked on the MB-SWCNTs adducts. It was worthy to note that DNA3/3DOM Au–Pd incubated for 1 h in buffer solution containing no Pb^{2+} resulted in almost negligible increase of the EIS signal (data not shown). These EIS results were in good agreement with the CVs results, as shown in Fig. S2B.

3.4. Experimental condition optimization

3.4.1. The concentration of MB in MB-SWCNTs adduct

The concentration of MB in MB-SWCNTs adduct was optimized based on the induced maximum current change. Upon the addition of 0.1 nM Pb^{2+}, the MB signal on the dsDNA modified 3DOM Au–Pd electrode enhanced rapidly with increasing the immobilized amount of MB in the MB-SWCNTs adduct. As shown in Fig. 3A, the current signal of MB rose with the immobilization time of MB on the surface of SWCNTs up to 40 min, then changed slowly, and finally reached a constant value at 60 min. So, 60 min was chosen as the optimum immobilization time.

3.4.2. The reaction time between DNA2 with Pb^{2+}

The reaction time between DNA2 with Pb^{2+} would have profound effect on the performance of the biosensor. Upon exposure to 0.1 nM Pb^{2+}, the cathodic peak current increased within 30 min of incubation and then remained constant when the reaction time was further elongated (Fig. 3B). So, an incubation time of 30 min was employed as the optimum reaction time between DNA2 with Pb^{2+}.

3.4.3. The hybridization time of DNA–MB-SWCNTs with DNA3

The hybridization time of DNA–MB-SWCNTs with DNA3 was optimized by the current response of MB-SWCNTs labels. As shown in Fig. 3C, the current value increased rapidly within 2 h and then continued to increase slowly. At time 2.5 h, the current value was stable without obvious change. Hence, 2.5 h was chosen as the optimal hybridization time.

3.4.4. The temperature effect on the DNA1 cleavage efficiency

The Pb^{2+} detection was performed by heating the Au–SiO_2@-Fe_3O_4 and MB-SWCNTs functionalized DNA1/DNA2 double strands to above 50 °C, and subsequently cooling it slowly to room temperature. At 50 °C, the substrate DNA1 and enzyme DNA2 were in the separated state because it was above the melting temperature of the DNA (T_m=46 °C) (Liu and Lu, 2004). The substrate cleavage occurred during the cooling process. Therefore, it was

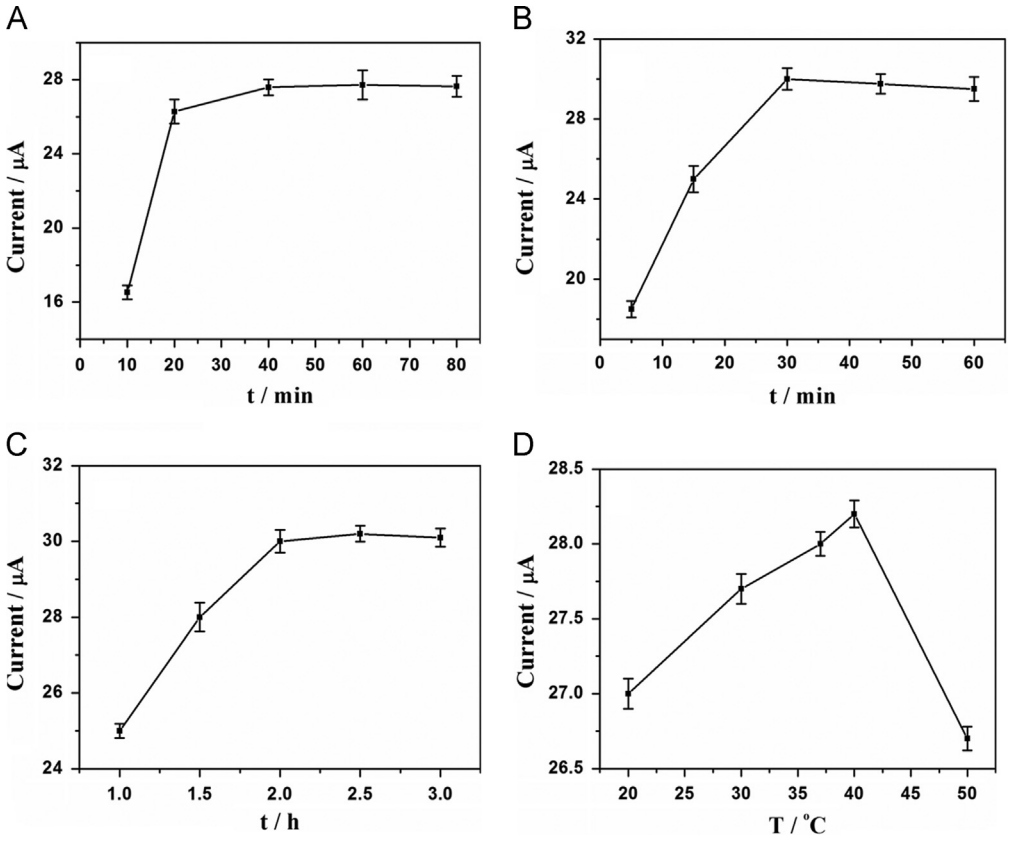

Fig. 3. The MB current signals on the dsDNA modified 3DOM Au–Pd electrode at different (A) immobilization times of MB, (B) reaction times between DNA2 with Pb^{2+}, (C) hybridization times of DNA–MB-SWCNTs with DNA3, and (D) experiment temperature, upon exposure to 0.1 nM Pb^{2+}. Electrolyte: 0.1 M pH 7.0 PBS+0.1 M KCl.

important to understand the temperature-dependence cleavage profile in the bio-nanocomposites functionalized system and to identify the temperature at which the cleavage was the most efficient. To this end, a sample of Au–SiO_2@Fe_3O_4 and MB-SWCNTs functionalized DNA1/DNA2 double strands was heated to 60 °C and allowed to cool to a predetermined temperature, at which point Pb^{2+} was added to the sample. The temperature was kept constant at that temperature for 10 min to allow the Pb^{2+} induced cleavage reaction to occur. At the end of the 10 min, EDTA was added to chelate Pb^{2+} and thus stop the reaction. Then the sample was heated to 60 °C again and cooled slowly to room temperature. A series of temperatures from 20 to 50 °C was tested, and the corresponding MB response currents are presented in Fig. 3D. As the temperature dropped below the melting temperature, the MB currents increased significantly. The fraction of substrate DNA1 cleaved reached a maximum at 40 °C, and then began to drop. Hence, 40 °C was chosen for Pb^{2+} detection and quantification.

3.5. Amperometric detection of Pb^{2+}

The binding of Pb^{2+} to DNA2 could unwind the double helix of DNA1 and DNA2, leading to the division of DNA1 into two fragments and the dissociation of DNA2. Then, the DNA–MB-SWCNTs part could hybridize with DNA3 on the 3DOM Au–Pd electrode, receiving the faradaic current response of MB. This target induced new strands hybridization strategy was expected to give a much larger signal change magnitude than the target-induced conformational change, in which the electrochemical events were usually recorded based on the distance alteration between the redox species and the electrode surface. Under optimal conditions, the dynamic range of the developed Pb^{2+} sensor was evaluated using DNAzyme-based MB-SWCNTs adduct as reporter probe and the 3DOM Au–Pd electrode as the sensing substrate. Fig. 4A shows that the DPV peak currents increased with the increase of Pb^{2+} concentration in the samples. Fig. 4B represents the linear relationship between the peak current changes (Δi_p) and the logarithm of target Pb^{2+} concentrations (log ($C_{Pb}{}^{2+}$)) in the range of 1×10^{-17}–1×10^{-4} M with a detection limit of 1×10^{-19} M at a signal-to-noise ratio of 3. The regression equation was $\Delta i_p = 40.6 - 2.0\log(C_{Pb}{}^{2+})$ ($n=6$), with the relative coefficient of 0.9864. Such a high sensitivity was attributed to the signal amplification of the 3DOM Au–Pd bimetallic substrate as well as the assembled numerous MB molecules for DPV response and the reducing background signal by the "signal-on" mode. Table S1 compares our present work with other latest DNAzyme-based biosensors for the detection of Pb^{2+} ions using fluorescence, ECL and electrochemical methods. The detection limit of our strategy is lower than that of other electrochemical and the fluorescence and ECL sensors for Pb^{2+}. The linear range of our strategy is wider than most of the other methods. Moreover, the electrochemical signal was reproducible, with coefficient of about 95% and 87% for target Pb^{2+}, when samples containing 0.1 nM and 1 pM Pb^{2+} were measured 5 times, respectively. The developed sensors could completely meet the requirement of water-quality and BLLs monitoring. This ultrasensitive detection of Pb^{2+} may be attributed to 3DOM Au–Pd film and the MB-SWCNTs adduct that can load more capture DNA3 and DNA2 molecules. In addition, 3DOM Au–Pd film and SWCNTs may serve as conducting tunnels or wires to improve the conductivity of the sensing system.

3.6. Specificity of the DNA biosensor

Specificity is an important factor to a sensor. The specificity of our designed strategy was evaluated by challenging it against

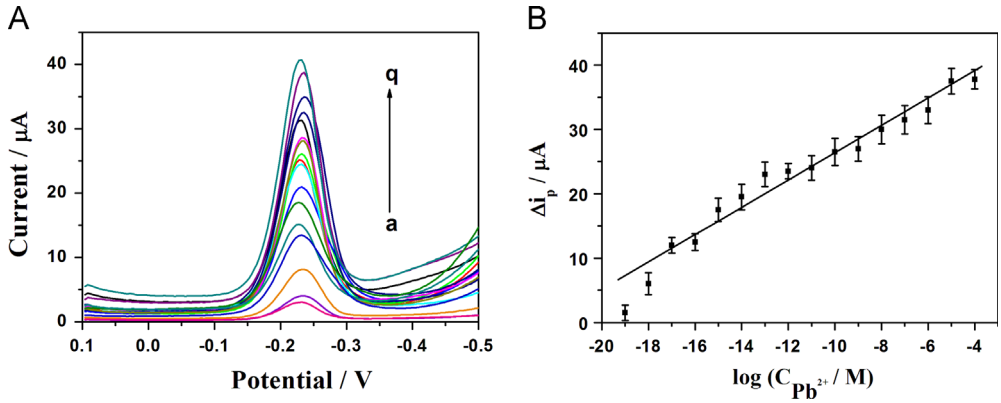

Fig. 4. (A) Typical DPV curves of the developed sensor in 50 mM Tris-acetate (0.5 M NaCl, pH 8.0) with different concentrations of Pb^{2+}: (a) 0, (b) 1×10^{-19} M, (c) 1×10^{-18} M, (d) 1×10^{-17} M, (e) 1×10^{-16} M, (f) 1×10^{-15} M, (g) 1×10^{-14} M, (h) 1×10^{-13} M, (i) 1×10^{-12} M, (j) 1×10^{-11} M, (k) 1×10^{-10} M, (l) 1×10^{-9} M, (m) 1×10^{-8} M, (n) 1×10^{-7} M, (o) 1×10^{-6} M, (p) 1×10^{-5} M, and (q) 1×10^{-4} M. (B) The linear relationship between the DPV peak current change and the logarithm of the concentrations of Pb^{2+}.

other metal ions including Mg^{2+}, Cr^{2+}, Zn^{2+}, Ca^{2+}, Cu^{2+}, Mn^{2+} Co^{2+}, K^{+}, Hg^{2+}, Fe^{3+} and Ni^{2+} (all at 0.1 nM). Fig. S3 shows histograms of faradaic current changes for the biosensor after reaction with various metal ions. Significantly, higher current change was observed with the target Pb^{2+} than those of other metal ions. The results clearly revealed that our DNAzyme sensor is well suited for selectively monitoring Pb^{2+} in the presence of other metal ions.

3.7. Reproducibility, stability and regeneration of the DNA biosensor

To further investigate the reproducibility of the as-prepared Pb^{2+} biosensor, we repeatedly assayed the Pb^{2+} ions with three different levels, using identical batch 3DOM Au–Pd electrodes, MB-SWCNTs adducts and Au–SiO_2@Fe_3O_4 composites. Experimental results revealed that the coefficients of variation (CVs) of the intra-assay between five runs were 3.8%, 5.2% and 4.6% for 0.1 fM, 0.1 nM and 0.1 μM Pb^{2+}, respectively (Fig. S4A). When the biosensor was stored at 4 °C over 3 weeks, the electrochemical response did not change obviously (CV 4.5%) for the detection of 0.1 nM Pb^{2+} solution (Fig. S4B). However, the CVs of the inter-assay with various batches were 7.3%, 6.8% and 8.6% towards the above-mentioned analytes, respectively. The low CVs indicated that the possibility of high-quality batch-to-batch preparation and excellent stability.

Reusability is also an extremely important feature for biosensors in the practical applications such as clinical diagnoses. In our test, the 3DOM Au–Pd electrode based DNA biosensor could be regenerated by incubating the hybridization of DNA3 and DNA–MB-SWCNTs modified electrode in hot water (90 °C) for 1 min, by which hybridized DNA was removed via thermal denaturation. After the regeneration procedure was performed five times, the DNA3-3DOM Au–Pd electrode almost retained its original hybridization efficiency, with the CV of 4.3% at the same Pb^{2+} concentration of 0.1 nM (Fig. S3C). The low CV represented that the developed strategy could be regenerated and used repeatedly.

3.8. Serum sample detection

With the rapid economic development in China, lead poisoning has increasingly become an important health risk factor for children and the workers engaged in the lead-related job. The practical use of the proposed biosensor was evaluated in serum samples. The same procedure was conducted for measurements by using serum samples without any pretreatments. The results are shown in Table 1, which compared the results with those obtained from the commercial automatic biochemical analyzer performed in JSCCL. These results indicated the presented method is in good agreement with the traditional clinical method. Thus, this method could satisfy the clinical need for detection of Pb^{2+} levels.

Table 1
Comparison of serum Pb^{2+} levels determined using the two methods ($n=5$).

Sample	Proposed method (μM)	Automatic biochemical analyzer	Relative deviation (%)
1	0.051 ± 0.002	0.053 ± 0.001	−3.8
2	0.050 ± 0.002	0.048 ± 0.001	+4.2
3	0.29 ± 0.012	0.31 ± 0.07	−6.4
4	0.36 ± 0.015	0.35 ± 0.08	−5.3
5	0.18 ± 0.008	0.19 ± 0.005	+2.8

4. Conclusions

The electrochemical DNAzyme based target-induced electronic switch for highly sensitive and selective detection of Pb^{2+} with the detection limit of 1×10^{-19} M, which was never reported by other methods. The main advantages of the present biosensor contributed to two aspects. First, the 3DOM Au–Pd electrode, MB-SWCNTs adducts and Au–SiO_2@Fe_3O_4 composites with high active surface area could enhance the immobilization of DNA molecules. Second, compared with the reported electrostatic adsorption of MB onto the capture DNA-functionalized electrode surface, the MB-SWCNTs adducts could only be immobilized on the electrode surface in the presence of Pb^{2+}, which decreased the blank signal significantly. Moreover, the biosensor was applied to determine Pb^{2+} in serum with satisfactory results. Importantly, by controlling the target probes with various metal ions-specific DNAzymes (such as Cu^{2+}, Mg^{2+} and Hg^{2+}), the assay can be easily extended for use with other metal ions and thus represents a versatile detection method.

Acknowledgments

We greatly appreciate the support from the National Natural Science Foundation of China (20905035) and State Key Laboratory of Materials-Oriented Chemical Engineering (KL10-15). This work is also sponsored by Qing Lan Project of Education Department of Jiangsu Province.

Appendix A. Supporting information

Supplementary data associated with this article can be found in the online version at http://dx.doi.org/10.1016/j.bios.2013.09.028.

References

An, L.L., Chang, Y.C., Du, J.Y., 2013. Chinese Journal of Applied Chemistry 30, 171–177.
Cai, L., Bahr, J.L., Yao, Y., Tour, J.M., 2002. Chemistry of Materials 14, 4235–4241.
Ceres, D.M., Udit, A.K., Hill, H.D., Hill, M.G., Barton, J.K., 2007. The Journal of Physical Chemistry B 111, 663–668.
Chen, X.J., Wang, Y.Y., Zhou, J.J., Yan, W., Li, X.H., Zhu, J.J., 2008. Analytical Chemistry 80, 2133–2140.
Chen, X.J., Zhu, J.W., Chen, Z.X., Xu, C.B., Wang, Y., Yao, C., 2011. Sensors and Actuators B 159, 220–228.
Chunglok, W., Khownarumit, P., Rijiravanich, P., Somasundrum, M., Surareungchai, W., 2011. Analyst 136, 2969–2974.
Dallaire, A.M., Rioux, D., Rachkov, A., Patskovsky, S., Meunier, M., 2012. The Journal of Physical Chemistry C 116, 11370–11377.
Datta, J., Dutta, A., Mukherjee, S., 2011. The Journal of Physical Chemistry C 115, 15324–15334.
Dong, H.F., Wang, C., Xiong, Y., Lu, H.T., Ju, H.X., Zhang, X.J., 2013. Biosensors and Bioelectronics 41, 348–353.
Gamero, M., Fierro, J.L.G., Lorenzo, E., Alonso, C., 2013. Electroanalysis 25, 179–188.
Gao, X.Y., Huang, H.M., Niu, S.Y., Ye, H.Z., Lin, Z.Y., Qiu, B., Chen, G.N., 2012. Analytical Methods 4, 947–952.
Gholivand, M.B., Azadbakht, A., 2012. Russian Journal of Electrochemistry 48, 457–466.
Hu, K.C., Lan, D.X., Li, X.M., Zhang, S.S., 2008. Analytical Chemistry 80, 9124–9130.
Huang, P.C., Su, P.H., Chen, H.Y., Huang, H.B., Tsai, J.L., Huang, H.I., Wang, S.L., 2012. Environment International 40, 88–96.
Imamura, K., Ikeda, E., Nagayasu, T., Sakiyama, T., Nakanishi, K., 2002. Journal of Colloid and Interface Science 245, 50–57.
Jusko, T.A., Henderson, C.R., Lanphear, B.P., Cory-Slechta, D.A., Parsons, P.J., Canfield, R.L., 2008. Environmental Health Perspectives 116, 243–248.
Kruger, K., Grabowski, P., Zaug, A., Sands, J., Gottschling, D., Cech., T., 1982. Cell 31, 147–157.
Li, H., Huang, X.X., Kong, D.M., Shen, H.X., Liu, Y., 2013. Biosensors and Bioelectronics 42, 225–228.
Li, J., Lu, Y, 2000. Journal of the American Chemical Society 122, 10466–10467.
Li, L.D., Chen, Z.B., Zhao, H.T., Guo, L., 2011. Biosensors and Bioelectronics 26, 2781–2785.
Liu, J.W., Lu, Y., 2004. Chemistry of Materials 16, 3231–3238.
Mawhinney, D.B., Naumenko, V., Kuznetsova, A., Yates Jr., J.T., Liu, J., Smalley, R.E., 2000. Journal of the American Chemical Society 122, 2383–2384.
Qian, P., Ai, S.Y., Yin, H.S., Li, J.H., 2010. Microchimica Acta 168, 347–354.
Sagara, T., Niki, K., 1993. Langmuir 9, 831–838.
Tang, S.R., Tong, P., Li, H., Tang, J., Zhang, L., 2013. Biosensors and Bioelectronics 42, 608–611.
Wei, N.N., Xin, X., Du, J.Y., Li, J.L., 2011. Biosensors and Bioelectronics 26, 3602–3607.
Wijnhoven, J.E.G.J., Zevenhuizen, S.J.M., Hendriks, M.A., Vanmaekelbergh, D., Kelly, J.J., Vos, W.L., 2000. Advanced Materials 12, 888–890.
Xiao, Y., Rowe, A.A., Piaxco, K.W., 2007. Journal of the American Chemical Society 129, 262–263.
Xu, G.L., Li, H., Ma, X.Y., Jia, X.P., Dong, J., Qian, W.P., 2009. Biosensors and Bioelectronics 25, 362–367.
Yan, Y., Zhang, M., Gong, K., Su, L., Guo, Z., Mao, L., 2005. Chemistry of Materials 17, 3457–3463.
Yang, T., Zhou, N., Li, Q.H., Guan, Q., Zhang, W., Jiao, K., 2012. Colloid Surface B 97, 150–154.
Yang, X.R., Xu, J., Tang, X.M., Liu, H.X., Tian, D.B., 2010. Chemical Communications 46, 3107–3109.
Yi, Q.F., Yu, W.Q., Niu, F.J., 2010. Electroanalysis 22, 556–563.
Yusuf, D., Zekerya, D., Gurel, N., Lo, G., 2005. Analytica Chimica Acta 542, 162–168.
Zhang, L.B., Zhu, J.B., Ai, J., Zhou, Z.X., Jia, X.F., Wang, E.K., 2013a. Biosensors and Bioelectronics 39, 268–273.
Zhang, X., Cao, Y., Yu, S., Yang, F.C., Xi, P.X., 2013b. Biosensors and Bioelectronics 44, 183–190.
Zhou, J.J., Huang, H.P., Xuan, J., Zhang, J.R., Zhu, J.J., 2010. Biosensors and Bioelectronics 26, 834–840.